Celia Martínez Soriano

EVALUATION OF OPTICAL TEMPERATURE SENSORS FOR MICROFLUIDIC CHIP APPLICATIONS

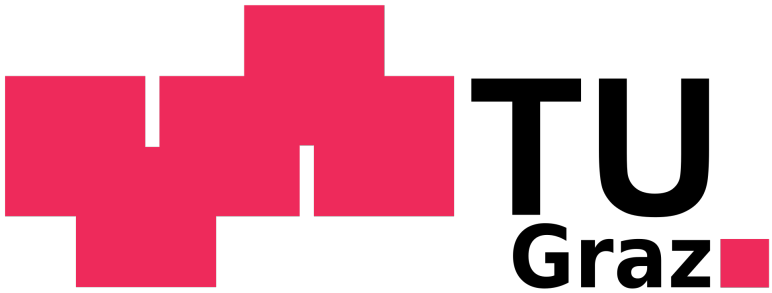

Institute of Analytical Chemistry and Food Chemistry
Technical University Graz
8010 Graz, Stremayrgasse 9/II

Head of the Institute: Ao.Univ.-Prof. Dipl.-Ing. Dr.techn. Erich Leitner

Tutor: Assoc. Prof. Dipl.-Chem. Dr.rer.nat. Torsten Mayr
Supervisor: Bernhard Müller

Graz (June, 2018)

Index

Introduction

Temperature is one of the most fundamental parameters in numerous processes, either in biological, physical or chemical ones. Focusing on applications involved in biomedical research, it should be highlighted that temperature is a physical property that governs every biological reaction within living cells. Either exothermic or endothermic reactions implicated in cellular functions occur at particular locations within a cell, which demonstrates that the temperature distributions inside a living cell reflect the thermodynamics and functions of the different cellular components. Therefore, it would be of great interest to achieve the ability of measuring accurately temperatures at this level. [1,2]

Temperature can be measured in many different ways, which are based on dilatation, bimetallic, Seebeck effect, etc. [3] The conventional thermometer, as based on the dilatation phenomenon, was invented in 1612 by the Italian physician Santorio Santorii. The bimetallic temperature sensor was invented late in the 19th century. It added a scale on the tube, which made it easier to see changes in temperature, but the system lacked precise units: the accuracy was about plus or minus 2 degrees. Then, in the 20th century the semiconductor temperature measurement devices were invented. Those respond to temperature changes with good accuracy but until recently lacked linearity. [4] Besides conventional thermometers, optical sensors are considered to be more attractive alternatives for sensing and continuously monitoring the temperature. They would enable the possibility of working on a cellular level [5], since they allow contactless and noninvasive measurements combined with high spatial resolutions and high temperature coefficients, which is hardly reachable with other methods. Optical measurements allow researching without disturbance or destruction of the sample and are also really easy to integrate. Thermocouple or carbon nanotube-based nanothermometers [6] are alternatives for temperature sensing with high spatial resolution and can overcome the limitations that present the optical sensors such as possible poor stability, UV excitation, poor quantum yields and toxicity.

The objective of this work is to evaluate optical temperature sensors for microfluidic chip applications. This includes building a measurement set-up, preparing different phosphorescent sensor spots, measuring calibration curves and their integration into microfluidic devices.

Microfluidic technology enables studies of cell behavior with precise and localized application of experimental conditions unreachable using macroscopic tools. For this kind of experiments, it is particularly important to find out if the conditions among the chip are the specified ones. Thus, it is necessary to corroborate if there exists a gradient of temperature in the chip and if its magnitude is big enough to affect the experiment that takes place in it. By selecting and pumping water into the chip at different flow rates we will find out from which one the experiments could start to be affected.

Theoretical foundation

Previous concepts

In an atom electrons are positioned in different orbitals, which are defined as regions in the space around the nucleus where there is a density of probability of finding them. These orbitals differ from each other in shape and energy. There are low energy orbitals and high energy orbitals. Electrons tend to occupy first, and whenever possible, the lowest energy orbitals if they are unoccupied. However, this does not mean that higher energy orbitals can not be temporarily occupied.

To move an electron from a low-energy level to a higher-energy one, it is necessary to cover that energy difference with an external source, usually in form of light. The energy difference between two given levels is mostly atom dependent, and the electrons can move between those orbitals only by winning or losing that specific amount of energy; each atom possesses its own absorption and emission lines. This process is known as electronic transition.

When atoms combine to form molecules, their atomic orbitals disappear and couple to form molecular orbitals. Electrons can now occupy regions of probability density around several nucleous. These combination of atomic orbitals occurs in a linear way. For example, if two atoms are combined, each having two atomic orbitals, the molecule has four molecular orbitals as a result. These molecular orbitals present energies with magnitudes in between to those of the atomic orbitals that were combined to form them.

Relatively simple molecules possess a very high number of molecular orbitals between which electronic transitions can occur. This is the reason why molecules have emission and absorption bands and not lines. These bands are constituted by superposition of a large number of lines corresponding to each of the possible transitions between different orbitals within the molecule.

There are various terms to describe the different shapes of lines inside the bands of absorption and emission. Normally, in a molecule in the ground state, many of the electrons are in the singlet state. Singlet is used to define a linked set of particles whose net angular momentum is zero, that is, whose overall spin number is zero. Therefore, there is only one spectral line in a singlet state. A doublet state presents one unpaired electron and “has” a doublet line splitting of spectral lines. Finally, a triplet state has two unpaired electrons and shows threefold splitting of spectral lines. Different “amounts” of energy are needed to move in between these spectral lines; it doesn’t take the same quantity of energy for an electron to jump from a singlet to another singlet state than in between the 3 lines of the triple state.

At last, it should be noted that the electrons of a molecule in the ground state are usually in the singlet state. [7]

Jablonski Diagram

A Jablonski diagram, **Figure 1**, is a simplified representation of the electronic (orbital) levels of a molecule and the possible electronic transitions that can occur between these levels. The electronic states are organized vertically according to their energy and horizontally according to their spin multiplicity.

An electronic excited molecule, in S1 level, can acquire a state of lower energy by different mechanisms. It can go through a 'non-radiative decay' in which most of the excitation energy is dissipated as heat (vibrations) to the solvent. They can also convert to a triplet state by delivering energy to another molecular orbital to obtain two orbitals with intermediate energies as final product, but this is actually a rare case and spin forbidden called “intersystem crossing”. [8]

Luminiscence

Luminiscence occurs when a molecule in its ground state absorbs the light energy carried by a single photon and is promoted to a higher-energy state, also named as electronically excited state. From there, the molecule undergoes vibrational relaxation and/or internal conversion in which some energy is dissipated. Then, from the lowest vibrational level in an excited electronic state, the molecule returns to its ground state by emitting a photon. Since the molecule has undergone a non-radiative decay, the emitted photon has less energy than the incident photon, which is an effect known as the Stokes shift. If we name as S_0 the ground state and S_1 the first singlet excited state, the excitation process can be expressed as

$$S_0 + h\nu \rightarrow S_1 \tag{1}$$

The emission process is expressed as

$$S_1 \rightarrow S_0 + h\nu' \tag{2}$$

In these equations h is Planck's constant and ν and ν' are, respectively, the frequency of the light of excitation or emission.

The Stokes-shift phenomenon is the result of two actions: vibrational relaxation and solvent reorganization. A fluorophore behaves as a dipole that is encircled by molecules of water. When it enters an excited state, its dipole moment changes, but water molecules are not able to adjust that quickly. The dipole moments realign only after vibrational relaxation. Thus, the light emitted during phosphorescence presents a lose of energy, quantized as

$$\Delta E = h(\nu' - \nu)\,, \tag{3}$$

And shows higher wavelengths than the excitation light since

$$\Delta\lambda = c\left(\frac{1}{\nu'} - \frac{1}{\nu}\right) > 0 \tag{4}$$

In the Jablonski Diagram (**Figure 1)** it can be seen that there are different luminescence deactivation pathways, when a photon is absorbed, such as

fluorescence, elastic/inelastic scattering, phosphorescence and vibrational relaxation. [8,9]

Phosphorescence (**Figure 1**) implies also an interaction with light. Fluorescence and phosphorescence differ in the emission times: Phosphorescent materials emit slowly light over time; while in fluorescent materials the light is emitted in shorter times. Since phosphorescence is related with spin forbidden transitions, it is unlikely to happen and therefore it is a slower process [10]:

$$S_0 + hv \rightarrow S_1 \rightarrow T_1 \rightarrow S_0 + hv' \qquad (5)$$

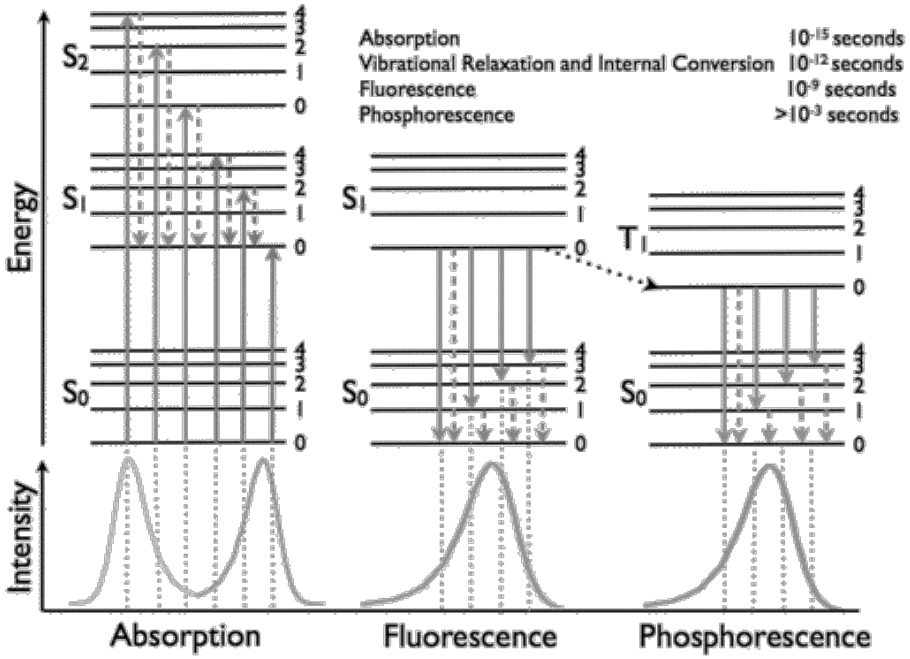

Figure 1. Jablonski diagram. Solid arrows indicate radiative transitions as occurring by absorption or emission of a photon. Dashed arrows represent non-radiative transitions. Internal conversion is a non-radiative transition, which occurs when a vibrational state of a higher electronic state is coupled to a vibrational state of a lower electronic state. [8]

Phosphorescence lifetime imaging (PLIM)

Phosphorescence Lifetime Imaging uses the detection of lifetime instead of phosphorescence intensities to obtain information on the environment of the phosphorescent material.

This technic can report on photophysical events that are difficult or impossible to observe by phosphorescence intensity imaging, because PLIM is independent of the local material concentration and excitation intensity. PLIM is used to image temperature, pH, refractive index and ion and oxygen concentrations, all at the cellular level. [11]

When trying to take images of phosphorescent sensors many different problems can occur. It can appear photobleaching of the applied dyes, light

scattering, background phosphorescence of the sample, non-homogenous fields of the light source, non-uniform distribution of the phosphorescent probes in the sample or the sensor layer and a varying thickness of the sensor layer.

As a solution to all the previously mentioned complications, PLIM registers the lifetime of the excited electronic state of a phosphorescent material, which is possibly the most attractive intrinsically referenced parameter. It allows the user to produce an image based on the differences in the exponential decay rate of the phosphorescence from a phosphorescent sample; an area is mapped in order to record possible heterogeneities or gradients and then it shows the results as images.

The decay of the phosphorescence intensity after a short pulse of light can be transcript in the form of

$$I(t) = I_0 \cdot e^{-t/\tau} \tag{6}$$

where $I(t)$ is the final intensity, I_0 the intensity when $t = 0$, and τ is the lifetime or decay time.

The following parameters of luminescence have to be taken into consideration: light intensity, wavelength, decay time, polarization, quantum yield and quenching efficiency.

PLIM can be detected in the frequency or in the time domain and the sample can be excited by a pulsed or a sinusoidal modulated light source.

The frequency-domain PLIM, **Figure 2 (left)**, consists on a technique of phase modulation. Sinusoidally modulated light is used to excite the sensor at a frequency that suits the decay time. Except for decay, the emission transmitted by the probe follows the modulation. The measurements of this difference are taken by quantifying the change of the phase angle between signals, the modulated signal and the emission signal. This phase shift of phosphorescence can be calculated using a detector with a gain modulator.

Once this phase-angle shift has been obtained, the decay time can be calculated in the following way:

$$\tau = \frac{\tan \Delta\phi}{2\pi f} \ , \tag{7}$$

where $\Delta\phi$ is the phase-angle shift and f the frequency of the sine modulation.

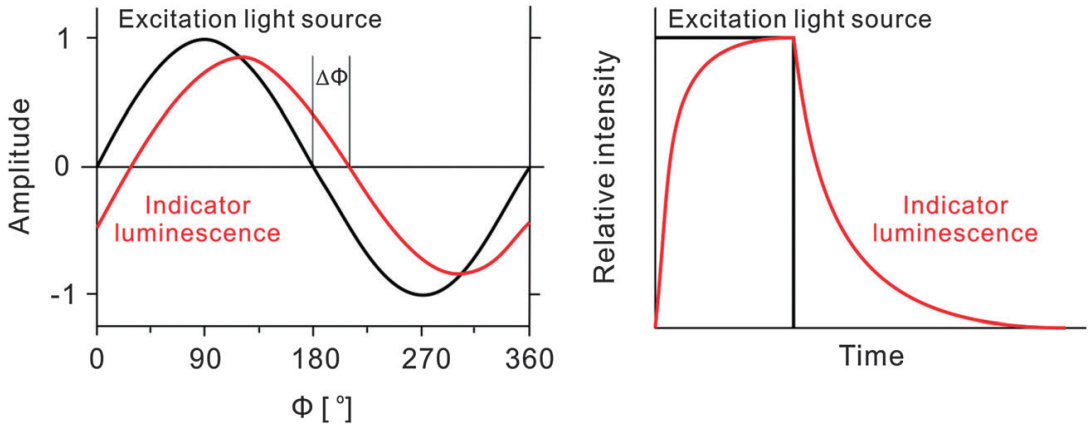

Figure 2. Schemes of frequency-domain (left) and time-domain (right) lifetime measurements. [12]

The time-domain PLIM, **Figure 2 (right) and Figure 3**, is based on the excitation by a LED pulse, in which the phosphorescence image is obtained by the gate operation of the image intensifier. It consists on the integration of various subsequent acquisition cycles of the images of two different gates. The image of each gate is shot separately. It is essential that the detector and the light source are pulsed at a similar magnitude frequency as the reciprocal decay time [12],

$$\tau = \frac{t_1 - t_2}{ln(A_1/A_2)}\ , \tag{8}$$

where t_1 and t_2 are the opening times of the separated gates, and A_1 and A_2 the areas covered by the emission function during the integration times.

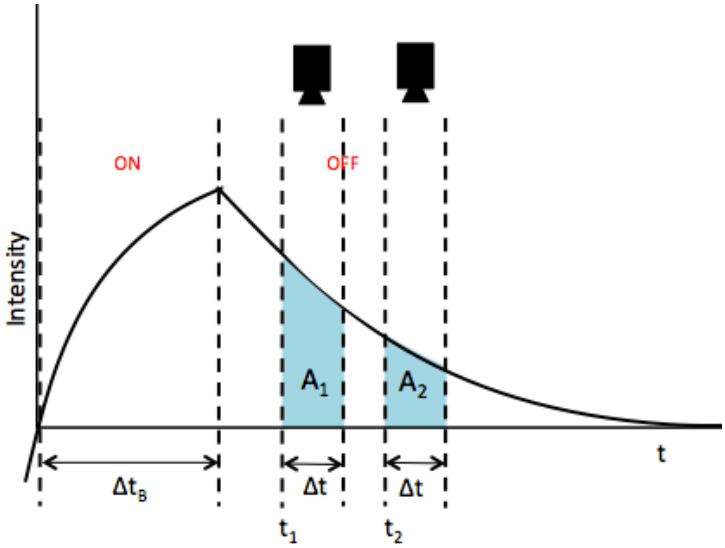

Figure 3. Time-domain approach. After a pulse of light, the detector is opened at times t1 and t2, corresponding to the first and the second time gate. They are open for an identical period of Δt. The lifetime is proportional to the ratio of the integrated photon counts A1 and A2.

PLIM supposes advantages in biomedical applications because the analysis of the sample doesn't involve its disturbance or destruction.

Materials and Methods

Indicator dyes

For sensing and imaging applications the following requirements are of primary importance:

- Good brightness (Product of molar absorption coefficient ε and luminescence quantum yield)
- Good photostability
- Adequate solubility in polymers to avoid aggregation after immobilization
- Large Stoke shifts, this way the emission can be efficiently separated from the excitation light [13,14]

Two different kinds of dyes were used for the production of the sensor foils: phosphorescent organic dyes and inorganic phosphor based dyes. The phosphorescent organic dyes selected were a dicyanobenzene based dye, which shows TADF (Thermally Activated Delayed Fluorescence) and a PdDBADCB dye and the inorganic phosphor based dyes chosen were the Egyptian Blue (EB) dye and the MgTiMnOn dye.

Dyes were not synthesized for the experiment, they were acquired. For further information about its synthesis:

- Dicyanobenzene based dye: Purely Organic Dyes with Thermally Activated Delayed Fluorescence—A Versatile Class of Indicators for Optical Temperature Sensing
- PdDBADCB dye: New Red-Emitting Schiff Base Chelates: Promising Dyes for Sensing and Imaging of Temperature and Oxygen via Phosphorescence Decay Time
- EB dye: The exceptional near-infrared luminiscence propierties of cuprorivaite (Egyptian Blue)
- MgTiMnOn dye: Mn4**+**-Doped Magnesium Titanate—A Promising Phosphor for Self-Referenced Optical Temperature Sensing

Organic dyes

$MgTiMnO_n$ presents the next features: straightforward synthesis, excellent chemical and photochemical stability of the inorganic phosphor and high temperature coefficients in the range 50°C to 150°C. The emission spectra for Mn^{4+} based dyes show a narrow peak at 660 nm and then a broad shoulder till 680 nm, **Figure 4 (a).** With any quantity of concentration of Mn^{4+}, the lifetime decreases as the temperature raises, **Figure 4 (b).** [15]

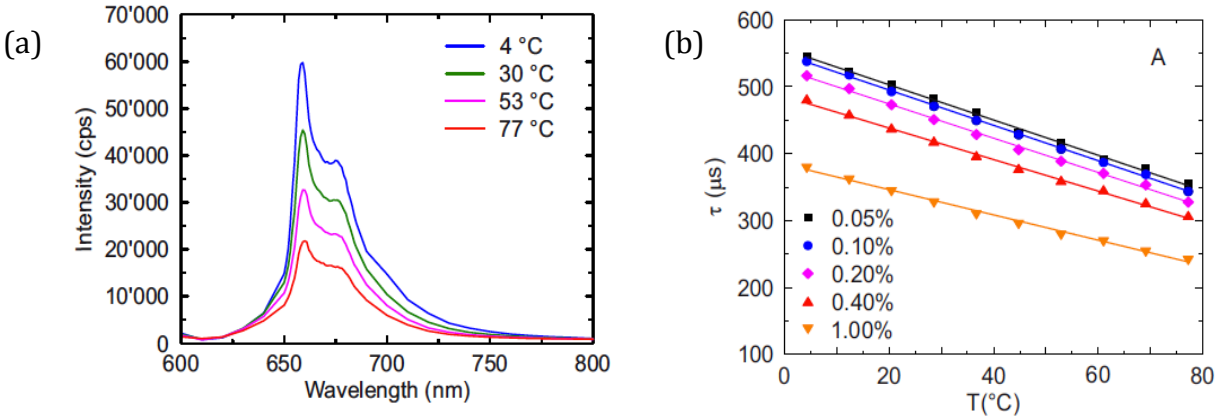

Figure 4. (a) Emission spectrum of the sample with a Mn4+ doping concentration of 0.40% at different temperatures and (b) Temperature dependence of the lifetime for samples with different Mn^{4+} doping concentrations. [15]

$CaCuSi_4O_{10}$ is the chemical formula of Egyptian Blue. This dye exhibits exceptional high emission quantum efficiency in the near-infrared region (λ=910 nm and ϕ>10,5%). It also presents a long excited lifetime. [16]

Inorganic phosphors

The **dicyanobenzene** based dye lifetime presents high temperature dependency, which seems to be very useful for designing advanced optical temperature probes. In **Figure 5** it is to see that ths Stoke Shift for different classes of TADF based dyes are very large.

The TADF (Thermally Activated Delayed Fluorescence) based temperature sensors demonstrate excellent sensitivity from −1.4 to −3.7% change of TADF lifetime per K, which favorably compares even to the highly sensitive optical thermometers reported in the literature. Moreover, it presents moderate decrease of brightness at higher temperature; in contrast to much stronger decrease of luminescence intensity observed for most of the state-of-the-art lifetime temperature probes. [17]

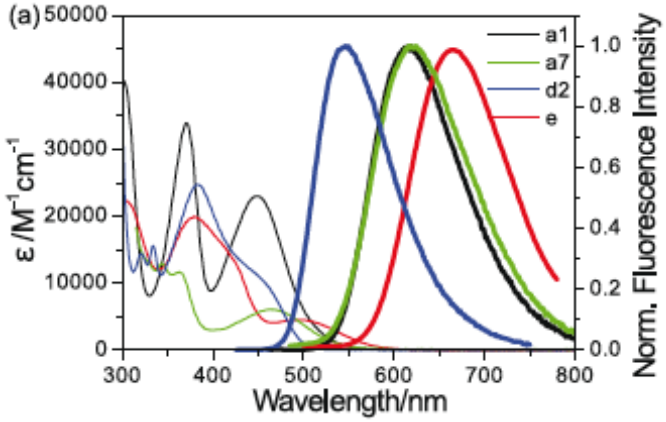

Figure 5. Absorption and emission spectra of different TADF based dyes at 25 °C; d2 corresponds to the dicyanobenzene based dye. [17]

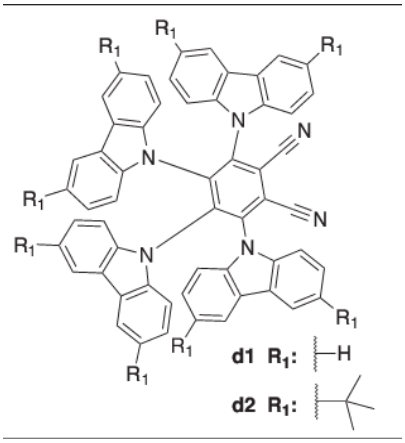

Figure 6. Chemical structure of the investigated TADF emitter; d2 corresponds to the dicyanobenzene based dye. [17]

PdDBADCB dye presents efficient absorption in the blue-green part of the spectrum with molar coefficients up to 98.000 $M^{-1}cm^{-1}$. Upon immobilization into the PViCl-PAN, its phosphorescence quantum yield increased from ϕ<1% to ϕ>10%. Considering the high molar absorption coefficients, the brightness of this material is high enough to enable sensing and imaging applications. The material also features remarkable photophysical properties such as room temperature phosphorescence and good photostability.

Phosphorescence intensity of the PdDBADCB dye is highly temperature-dependent and an almost linear decrease of the intensity with temperature is observed, **Figure 7(a)**. In addition, the temperature coefficients of the decay time are reported to be among the most sensitive ones in literature so far. [18]

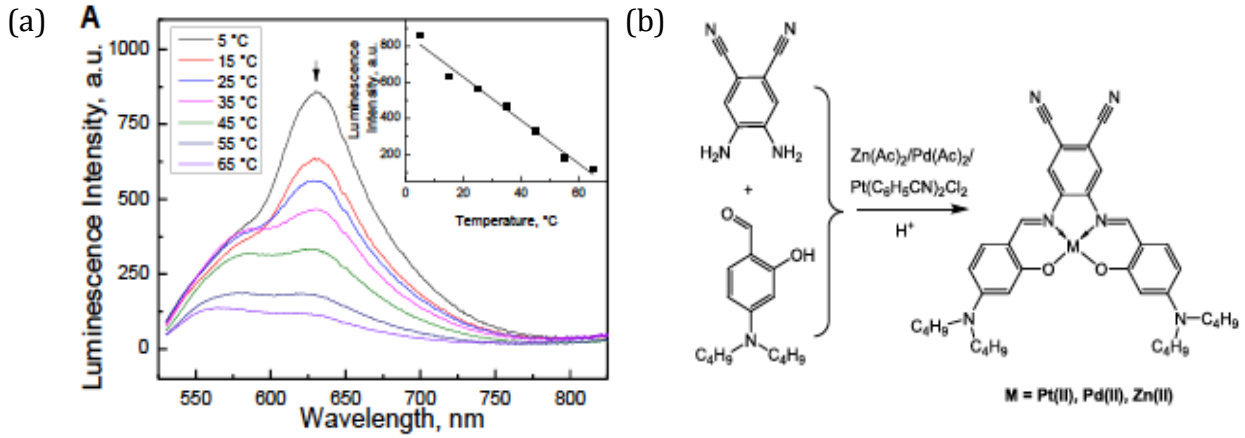

Figure 7. (a) Temperature-dependency of the emission spectra of PdDBADCB based dye immobilized in PViCl-PAN and (b) its chemical structure. [18]

Sensor composition

Sensor layer

Immobilization of dyes in polymers is an essential aspect for their application in optical temperature sensing. The MgTiMnOn and the EB dyes were immobilized in moderately oxygen-permeable polystyrene (PS) as they are ceramic bulk materials and insensitive to oxygen. For the dicyanobenzene based dye and the PdDBADCB dyes virtually gas-permeable poly (vinylidene

chloride-co-acrylonitrile) (PViCl) was chosen for its immobilization due to the fact that both of them are cross-sensitivity to oxygen.

To make the ceramic ”dye” cocktails, THF (90%) was used as solvent with the PS (10%). For the MgTiMnOn a propotion of (2:1) to the PS solution was followed and for the EB it was used a proportion of (1:1) to the PS solution.

For the oxygen-sensitive ”dye” cocktails were needed special conditions. All the process was pursued inside a M. Braun Inertgas-Systeme glove box (www.mbraun.com) with special conditions of no oxygen, no humidity, normal pressure (±15 mbar) and temperature. THF was added as solvent. A 0,5% PdDBADCB in PViCl-PAN “dye” cocktail and a 0,5% dicyanobenzene based “dye” cocktails were obtained.

Cover layer

To enhance the intensity of the signal that’s is going to be capted, different types of coating materials on the sensitive material were used.

- P170(TiO_2) in silicon E_4
- 10 % PS in THF/Toluene

For the production of the silicon layer n-Heptan was used as solvent. The proportions were TiO_2 (2:1) E4 and n-Heptan (3:1) E4. For the polystyrene (PS) based layer THF/Toluene was used as solvent in a (2:1) proportion.

Sensor foil fabrication

Knife coating of the sensor layer

The prepared “dye” cocktails were knife coated with a 3 milli-inche (76 µm thicknes) wet film knife (www.byk.com) onto 125 µm biaxially oriented polyethylene terephthalate (PET) foils (MELINEX 506) supplied by Pütz GmbH + Co. Folien KG (www.puetz-folien.com).

For the organic dyes all the process was carried under normal ambient conditions, but for the inorganic dyes the knife coating was pursued inside a M. Braun glovebox (www.mbraun.com) and after the evaporation of the solvent, the foils were retrieved from the glove box.

Knife coating of the cover layer

The TiO_2 in E4 was knife coated with a 1 milli-Inche (25, 3 µm) wet film knife on the sensor foil and the 10 % PS was knife coated with a 3 milli-Inche (76 µm) knife on the backside of the sensor foil. While the coating was being performed with the knife, the foil was fixed to the glass with water so it didn’t move. The goal was to apply the layers onto the foil as homogenous and uniform as possible, so scattering could be avoided and the signal absorption increased.

Fabrication of microfluidic chip

A rhombic chamber chip-250 µL chamber volume (Product code: 12-0915-0194-01; Lab-on-a-Chip Catalogue 09/2012 , Microfluidic chipshop) of PMMA was used for the performance of the experiment, **Figure 8(a)**.

Dimensions:

- Volume: 250 µL
- Depth: 800 µm
- Lid thickness: 175 µm
- Critical dimesion: 7,04 mm^2

We arranged three equidistant spots of the most sensitive dye, PdDBADCB in PViCl-PAN, on the top of the channel of the chip and three equidistant spots on the bottom of the channel, in a way that they don't overlap, **Figure 8 (b).**

- PdDBADCB + TiO2 in E4 is located on the top of the channel
- PdDBADCB + PS is located on the bottom of the channel

The spots were extracted from the foils with a diameter of 3 mm by a Secabo Lapos laser cutter (www.secabo.com). To unit the spots to the chip, a little drop of E4 silicone was placed inbetween and pressure was exerted until it stuck. Finally, everything was covered with a sheet of the same material as the chip as a fixing and protection cover.

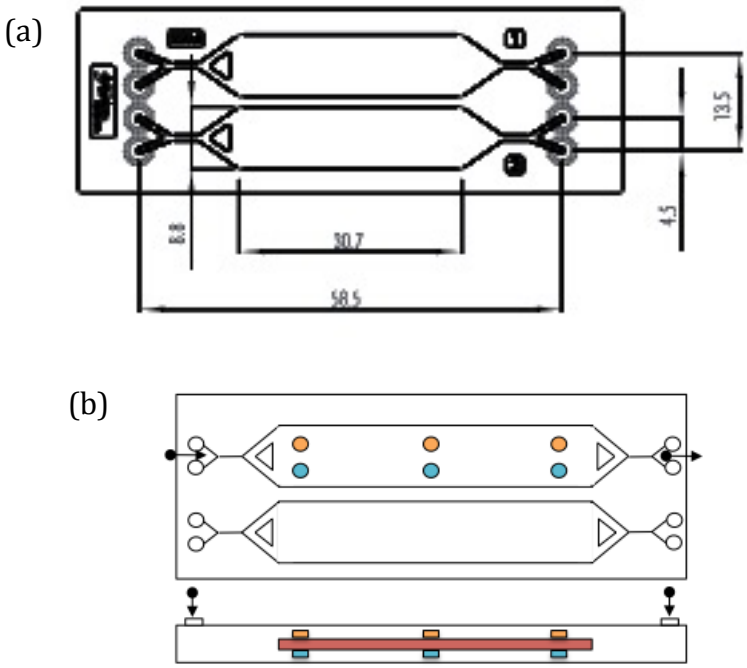

Figure 8. (a) Schematic drawing of the rhombic chamber chip-250 µL chamber volume [19] and (b) schematic drawing of the position of the measurement spots and the direction of the water flow.

Experimental Set-Up

In this work, two temperature measurement methods were used: imaging method and phase-angle method.

Lifetime imaging (time-domain)

Imaging of the phosphorescence lifetime of various temperature sensitive dyes was performed with a time-gated and electrically cooled CCD-camera (PCO Sensicam from Computer Optics, www.pco.de) via rapid life determination (RLD) equipped with a Pentax TV Lens 12 mm 1:1.2 lens. CCD-based imaging allows the measurement of various samples with just one independent image analysis. The CCD-Chip is formed by a 2D-array of pixels each representing a different point of the sensor. The sensor absorbs and then emits a light signal, following the principles explained for the phosphorescence, which is going to be detected by the pixels. Then, the light intensity is converted into a gray scale value, **Figure 9**.

For the camera an f-number of 2 was settled to achieve an optimal focus of the microfluidic chip channel and a sufficient luminescence signal from the sensor.

Using a short light pulse the phosphorescent material was excited. After a delay to cut of excitation light, the emitted signal is detected during two separate time gates. The lifetime is calculated, according to **Eq. (8)**, from the pixels gray values captured during these two gates, A1 and A2, and the times of the start of the two gates, t_1 and t_2.

Fixed filters are used to isolate the excited and emitted wavelengths. In the experiment we work with:

- Combination of GG495 Filter (www.leefilters.com) and Lee Oklahoma Yellow Filter (www.leefilters.com) for the dicyanobenzene in PviCl-PAN, the MgTiMnOn in PS and the PdDBADCB in PviCl-PAN dyes.

- RG9 Filter (www.leefilters.com) for the EB in PS dye.

As the excitation light source, a blue (λ=455 nm) and a red (λ=625 nm) high power LED array (OSRAM Oslon SSL 80) were utilized. The blue one was used for the dicyanobenzene in PviCl-PAN, the MgTiMnOn in PS and the PdDBADCB in PviCl-PAN dyes and the red one for the EB in PS dye.

The original settings used in the imaging method were:

- LED excitation time: 50 µs
- Windows gate time: 10 µs
- Time between the LED excitation time and the opening of the first window gate: 1 µs
- Time between the first and the second window gates: 1 µs

- Integration time: 30 ms

The values of each of the settings have been chosen so that the difference of gray level between the pixels of gate 1 and gate 2 is sufficient for the lifetime calculation. Looking at **Eq. 8**, it is to see that if the values are very similar there is no way to proceed with the measurement. It is necessary toreach a compromise between the windows gate time and the time between the first and the second window gates with the integration time. Increasing the first ones will help to create a difference between gate 1 and gate 2 values, but the integration time of the entire system will be reduced.

For the dicyanobenzene in PViCl-PAN the PdDBADCB in PViCl-PAN and the EB in PS these setting were suitable, but for the MgTiMnOn in PS settings had to be changed due to its longer lifetime. It was necessary to adjust the integration time to 160 µs and the time between the first and the second window gates to 75 µs.

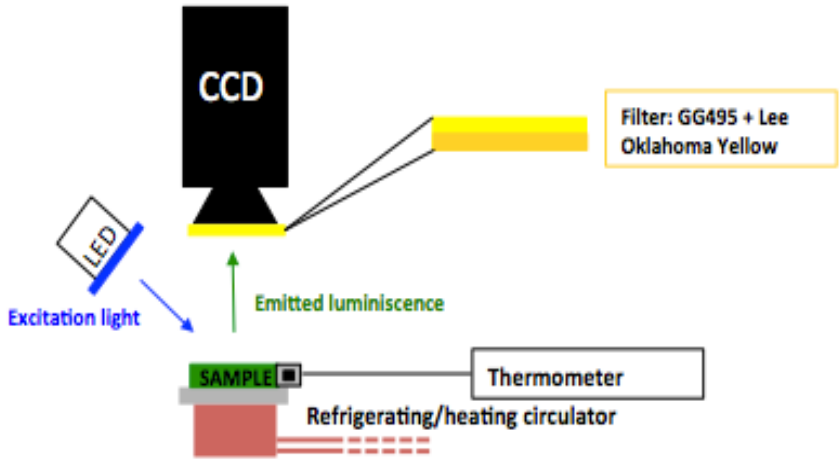

Figure 9. Experimental set-up a) for the temperature imaging method

Lifetime measurements (frequency domain)

The measurements done with the **phase-angle method** were performed with a compact USB-powered phase-fluorimeter from Pyro Science (www.pyro-science.com). The OEM modul was customized with a 465 nm excitation LED, Linos DT-cyan dichroic mirror and the Schott OG 590 long-pass filter used in combination with a Deep olden Amber plastic filter from Lee filters (www.leefilters.com), **Figure 10**. For EB in PS the standard device Firesting from Pyroscience (λ_{ex}=620 nm) was used. The phase-angle is obtained and from this one, following **Eq. (9)**, lifetime is measured.

The settings used in the phase-angle method were:

- Led intensity: 100%
- Amplification: 400x
- Oxygen Measuring Time: 90 ms
- Frequencies:

- Dicyanobenzene in PViCl-PAN (8kHz)
- PdDBADCB in PViCl-PAN (2kHz)
- EB in PS (2kHz)
- MgTiMnOn in PS (400Hz)

High intensity signal values were searched so that there was the minimal possibility of error and also a Stoke shift long enough that it allows the differenciation between the excitation signal and the emission signal.

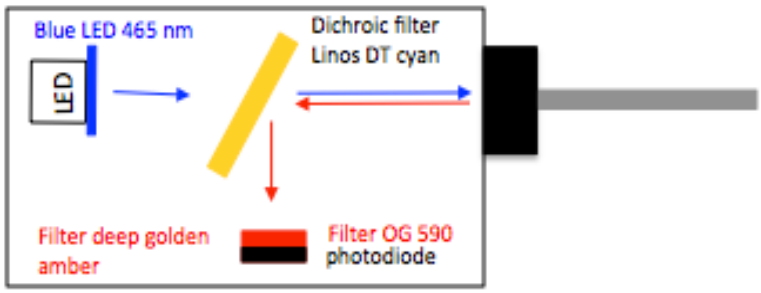

Figure 10. Experimental set-up for the temperature phase-angle method.

Calibration

Calibration of sensor material

To calibrate the sensor materials a cooling/heating device was used to temperate the the sensor foils to 7 different temperatures: 10°C, 20°C, 25°C, 30°C, 35°C, 40°C and 50°C. Then, both measurement methods were used, the imaging method and the phase-angle method, and a linear adjustment was made for each of the methods for each of the materials.

Calibration of microfluidic chip

To calibrate the microfluidic chip a cooling/heating device was used to temperate the the sensor foils to 7 different temperatures: 10°C, 20°C, 25°C, 30°C, 35°C, 40°C and 50°C. Water was inserted with a syrange into the chip's channel but without flow; the water was not circulating along the channel. Then, both measurement methods were used, the imaging method and the phase-angle method, and a linear adjustment was made for each of the methods for each of the spots.

Chip measurements

To check the possible existence of a gradient of temperature in the microfluidics chip, the following set-up was implemented. A cooling/heating device was and to make sure what the right temperature values were achieved, a temperature potenciometric (PT100 Element) sensor (High Precision Digitalthermometer, GMH 3750) was placed on the base plate, right next to the location of the chip, see **Figure 4**. With the help of a 3D printer, a removable cover is designed for the upper part of the chip, so that it allows us to achieve

certain isolation from ambient temperature and to place the optical fiber used by the phase-angle method always precisely on the same position.

A temperature of 37°C was stabilished constantly. Microfluidic chips are usually used for cell experiments and it is important to know how they behave with normal body temperature. Water was pumped through the channel of the chip with a syringe pump (Aladdin Single-Syringe Pump, www.wpiinc.com) to see the effect in the temperature for different flowrates.

Flow rates of 2,5 µL/min, 25 µL/min, 75 µL/min and 500 µL/min were settled. This way, it is possible to see if there exists some temperature gradient along the chip taking into consideration the different flowrates. The water is pumped into the chip at a normal room temperature and it is warmed with the heater when it enters in the chip.

The original settings used in the imaging method were:

- LED excitation time: 50 µs
- Windows gate time: 10 µs
- Time between the LED excitation time and the opening of the first window-gate: 1 µs
- Time between the first and the second window-gates: 1 µs
- Integration time: 30 ms

The setting used in the phase-angle method were:

- Led intensity: 100%
- Amplification: 400x
- Oxygen Measuring Time: 90 ms
- Frequency: PdDBADCB in PViCl-PAN (2kHz)
- Manual Background Compensation: 5,46 mV

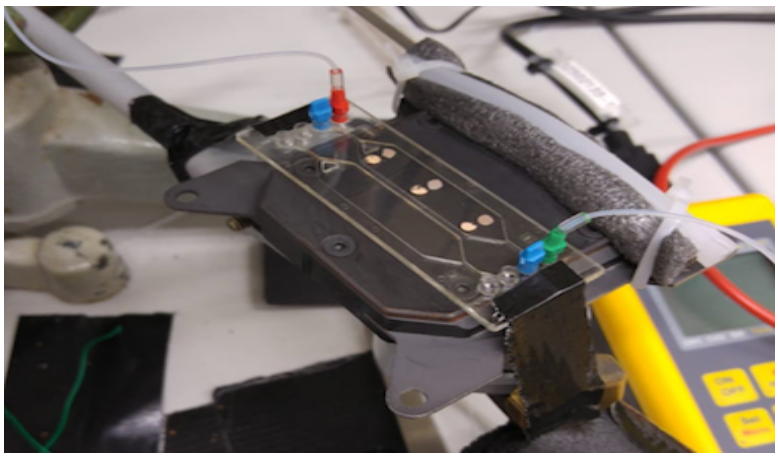

Figure 11. Picture of the pumping set-up without the isolation cover.

Results and discussion

Selection of the dye

It has been founded out the lifetime of the sensing materials using two different methods, the imaging and the phase-angle ones.

Table 1 contains the lifetimes of the different dyes in percent with the temperature and the value of the lifetime for 37 °C. It is important to highlight this particular temperature, because it is the one at which biological experiments will be carried out.

As it can be seen in **Figure 12-16,** the sensitivity of the measurement for the different materials is quite similar in between the methods. Taking as 100% the value obtained with the phase-angle method, **Table 1**, and comparing materials, it is possible to see how different the methods are between each other. For the dicyanobenzene based dye we perceive a difference of 14% , for the PdDBADCB in PViCl-PAN of 26%, for the EB in PS of 29% and for the MgTiMnOn of 28% approximately. We find the less significant differences for the dicyanobenzene dye and for the PdDBADCB dye, **Figures 12-16**. An explanation for the variance between methods can probably be that in this experiments no compensated background of the phase fluorimeter was used.

The less significant differences are founded for the dicyanobenzene based dye and for the PdDBADCB dye, see **Figures 12 to 16**. It also should be noted that it is easy to discover that there is an outliner in the measurement of the MgTiMnOn, specifically for the value obtained at 25 °C, **Figure 6**; without this value the sensitivity turns out be -0,51 instead of -0,39, which represents a great similarity between methods.

Regarding the values of the standard deviation (std), **Tables 2** and **3**, the phase-angle method seems more reliable for its results, but it is difficult to affirm this, since the signal intensities for this method were very low. The values of standard deviation obtained for each material in the imaging method are quite large. For the selection of the material and the subsequent analysis of the results, it should be taken into account that this method is less rigorous than the other.

For both processes, the aquired results, **Table 1** and **Figure 14**, showed that the dye with higher sensitivity to temperature and, therefore more significant for our study, was the PdDBADCB in PViCl-PAN. It achieved a sentivity of -2,62 for the imaging method and -2,08 for the phase-angle one, which would be double of the one obtained for the next highest one.

	Phase-angle method			Imaging method	
Dye	**ν (Hz)**	$\tau(\%)/T$	**τ [µs] at 37°C**	**τ [%/°C]**	**τ [µs] at 37°C**
Dicyanobenzene	8000	-1,04	3,80	-1,19	8,96
PdDBADCB	2000	-2,08	37,55	-2,62	40,58
EB	2000	-0,20	116,39	-0,26	123,88
MgTiMnOn	400	-0,55	285,29	-0,51	231,80

Table 1. Comparison of the photophysical properties of the dyes obtained with the frequency-domain/phase-angle method and the time-domain/imaging method.

	Lifetime + std (µs)			
Temp. (°C)	**Dicyanobenzene**	**PdDBADCB**	**EB**	**MgTiMnOn**
10	4,89±0,11	58,68±0,04	122,64±0,01	327,50±0,06
20	4,45±0,08	51,09±0,02	120,27±0,02	314,30±0,02
25	4,25±0,14	46,69±0,01	119,23±0,01	305,87±0,02
30	4,11±0,10	43,50±0,03	117,89±0,01	296,06±0,02
35	3,86±0,05	40,32±0,02	116,88±0,02	286,46±0,07
40	3,67±0,02	35,58±0,03	115,89±0,01	278,75±0,09
50	3,30±0,05	27,17±0,02	113,42±0,01	267,28±0,02

Table 2. Values of the lifetime and standard deviation for the phase-angle method.

	Lifetime + std (µs)			
Temp. (°C)	**Dicyanobenzene**	**PdDBADCB**	**EB**	**MgTiMnOn**
10	11,89±0,24	72,42±5,72	131,21±27,58	264,03±24,03
20	10,72±0,21	58,86±3,92	130,58±28,76	263,55±23,89
25	10,18±0,21	53,11±3,36	128,38±26,32	202,50±18,97
30	9,65±0,18	46,99±2,58	126,84±26,00	245,49±21,02
35	9,15±0,17	42,59±2,19	124,18±25,81	239,30±21,95
40	8,75±0,18	38,25±2,09	124,95±26,24	238,30±21,48
50	7,81±0,16	29,78±1,43	118,44±24,66	219,36±19,50

Table 3. Values of the lifetime and standard deviation for the imaging method.

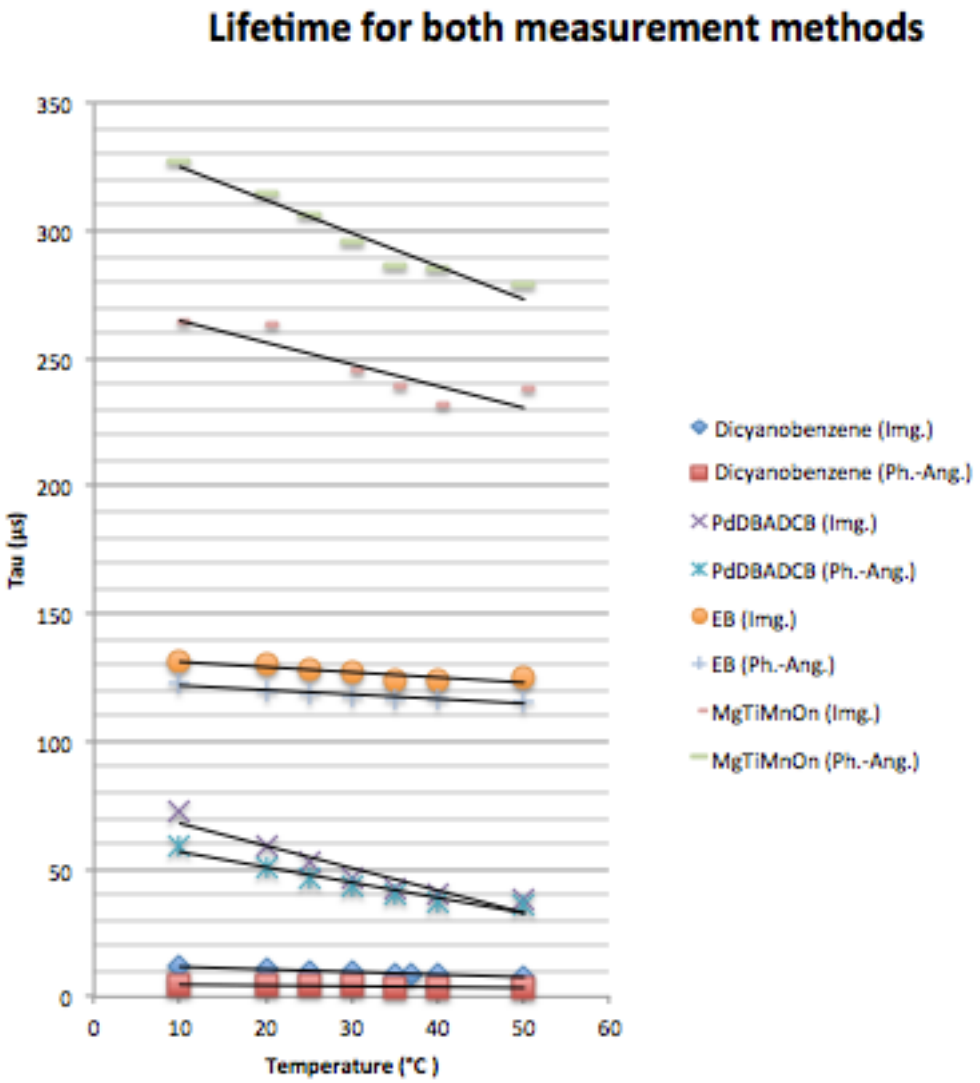

Figure 12. Overview of the lifetime obtained for the different dyes and temperatures with the time-domain/imaging method and the frequency-domain/ phase-angle method.

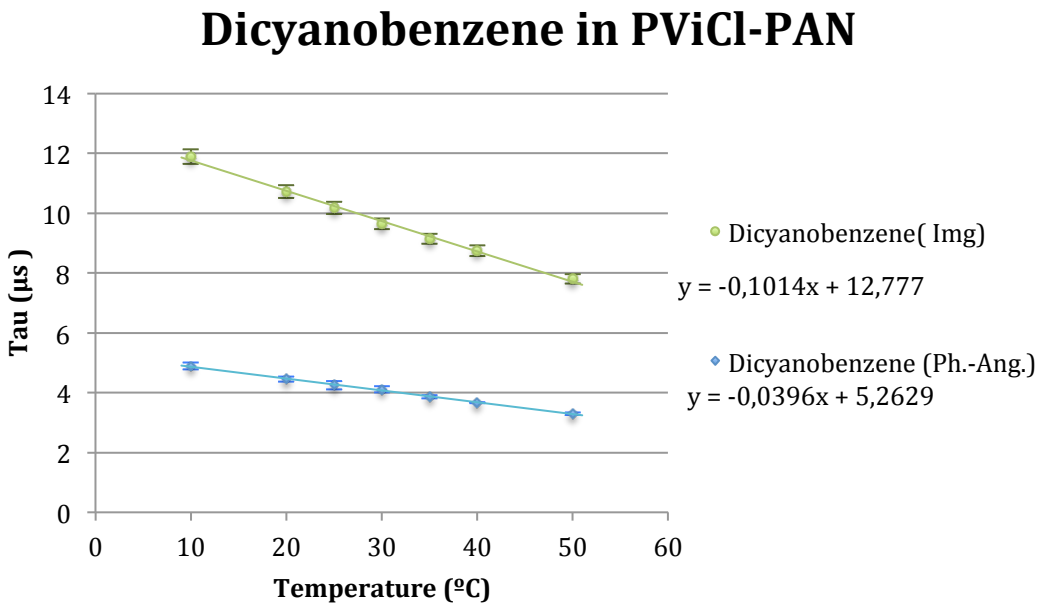

Figure 13. Comparison of the lifetime and standard deviation obtained for the dicyanobenzene based dye with the time-domain/imaging method and the frequency-domain/ phase-angle method.

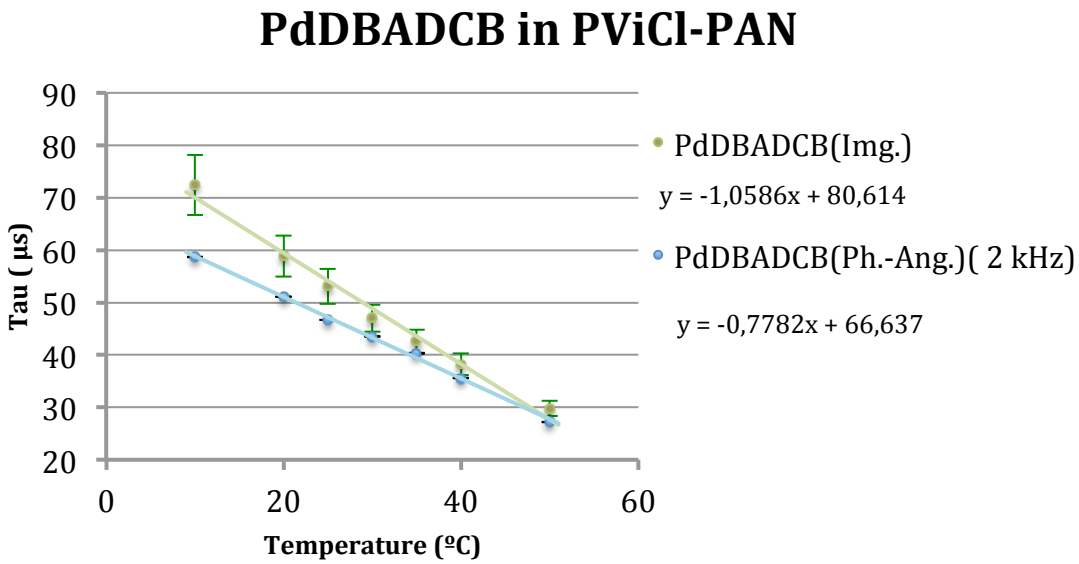

Figure 14. Comparison of the lifetime and standard deviation obtained for the PdDBADCB dye with the time-domain/imaging method and the frequency-domain/ phase-angle method.

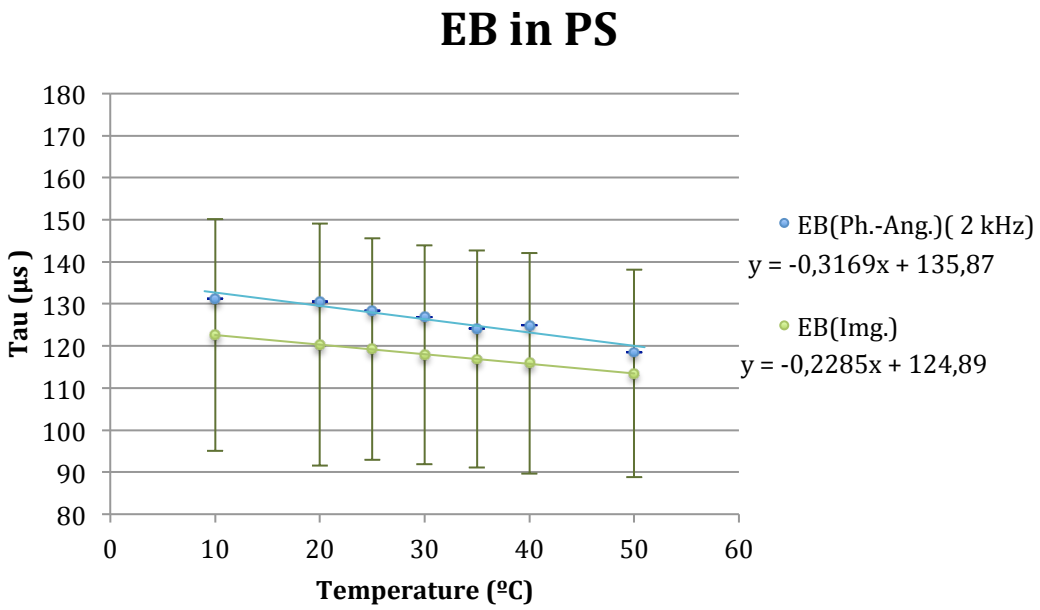

Figure 15. Comparison of the lifetime and standard deviation obtained for the EB dye with the time-domain/imaging method and the frequency-domain/ phase-angle method.

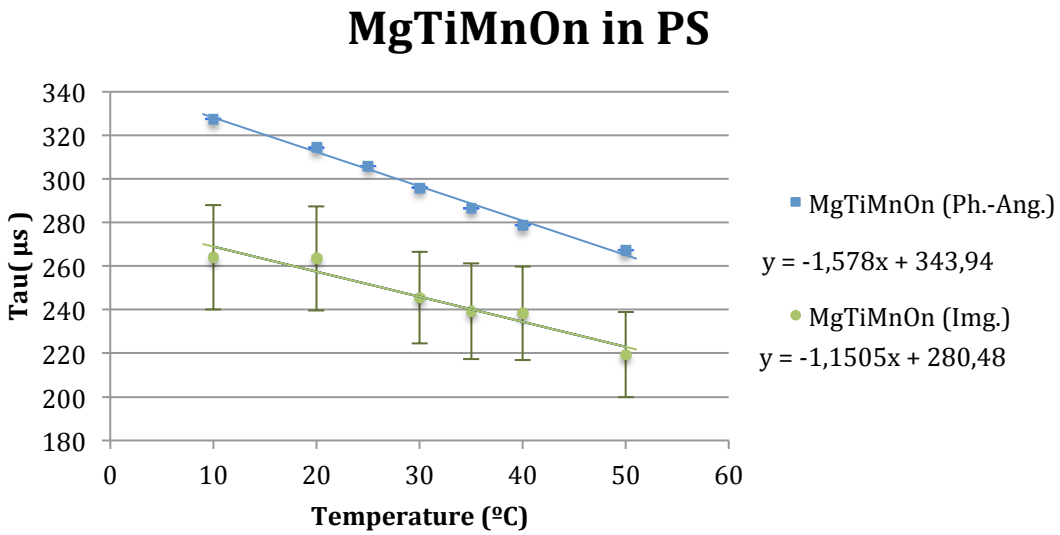

Figure 16. Comparison of the lifetime and standard deviation obtained for the MgTiMnOn dye with the time-domain/imaging method and the frequency-domain/ phase-angle method.

Chip calibration and flowrates results

As the PdDBADCB + PS is located below the channel and the PdDBADCB + TiO2 in E4 is located on the top, it is normal to expect higher temperatures for the PS ones than for the TiO2 In E4, as one is closer to the heater than the other.

It is to see, **Figures 17-18**, that τ reduces its value as the temperature grows. In the case of the PdDBADCB + TiO2 in E4, **Table 4** and **7**, the trend line does not vary between the measuring methods. However, in the case of the PdDBADCB + PS, **Table 4 and 7**, there is an acquisition of higher values of τ

with the phase-angle method than with the imaging method. Maybe it is because of the lower values of signal intensity.

It is remarkable, that for both cover layers, the slope of the adjusted linear function $\tau/T(°C)$ provided by the imaging methods seems to have a higher similarity than the phase-angle one**, Figure 17-18.** Focusing on the sensitivity to temperature, $\tau(\%)/T$ in **Table 4**, there are no differences higher than 10% in the values of each coating for each method. If we compare between methods, the disparity increases up to 20% in the case of PdDBADCB in PviCl + PS and 10% in the case of PdDBADCB in PviCl + E4. Finally, if we compare between the coatings, between the PdDBADCB in PviCl + PS and the PdDBADCB in PviCl + E4 for the phase-angle method we find differences of about 60% and 40% for the imaging method.

Although the trend line is similar, it is to see that for PdDBADCB in PViCl-PAN + PS we obtain higher values of τ for the same temperatures than for the PdDBADCB in PViCl-PAN + TiO2 E4.

Analyzing the values of the standard deviation, **Table 5** and **6**, we find that the phase-angle method shows more accurate results. A standard deviation of 2-10 μs can help the possible conclusions attainable from the study. If we have $\tau \approx 38\ \mu s$, the deviation supposes variations from 5%-25% approximately. This high deviation values could appear because of a bad selection of the area of interest when doing the calibration.

		Phase-angle method			Imaging method	
Dye	**Layer cover**	**Spots**	$\tau(\%)/T$	**τ [μs] at 37°C**	$\tau(\%)/T$	**τ [μs] at 37°C**
PdDBADCB	PdDBADCB + PS (TOP)	1	-1,94	41,22	-2,29	38,29
		2	-1,92	41,97	-2,37	38,23
		3	-1,81	41,79	-2,26	37,82
	PdDBADCB + TiO2 in E4 (BOTTOM)	1	-2,87	36,86	-3,17	36,77
		2	-2,85	37,09	-2,96	37,36
		3	-2,75	37,18	-3,11	38,23

Table 4. Comparison of the photophysical properties of the PdDBADCB in PViCl-PAN dye with different cover layers obtained by the frequency-domain/phase-angle method and the time-domain/imaging method.

	Lifetime + std (µs)					
	PdDBADCB + TIO2 in E4 (TOP)			PdDBADCB + PS (BOTTOM)		
Temp. (°C)	SPOT 1	SPOT 2	SPOT 3	SPOT 1	SPOT 2	SPOT 3
48,36	24,53±0,08	25,26±0,06	24,12±0,03	30,49±0,06	30,8±0,09	30,81±0,06
39,10	35,48±0,06	36,35±0,05	38,39±0,08	44,56±0,14	45,83±0,18	46,22±0,16
34,42	38,89±0,04	39,20±0,03	40,47±0,04	43,48±0,04	44,21±0,14	43,87 ±0,07
29,72	44,73±0,07	44,5±0,03	44,05±0,04	44,99±0,05	45,61±0,10	45,5±0,05
25,10	49,18±0,07	49,58±0,04	49,63±0,04	49,06±0,06	50,49±0,07	49,04±0,08
20,35	54,10±0,05	55,64±0,02	55,15±0,03	56,28±0,11	57,00±0,08	49,04±0,14
11,01	69,87±0,02	67,29±0,04	63,66±0,01	62,53±0,03	63,22±0,11	61,96±0,08

Table 5. Values of the lifetime and standard deviation for the phase-angle method.

	Lifetime + std (µs)					
	PdDBADCB + TIO2 in E4 (TOP)			PdDBADCB + PS (BOTTOM)		
Temp. (°C)	SPOT 1	SPOT 2	SPOT 3	SPOT 1	SPOT 2	SPOT 3
48,36	23,82±2,30	23,90±2,59	25,17±2,46	28,59±2,94	29,15±2,78	28,39±2,58
39,10	37,48±3,78	37,87±3,15	36,39±4,25	39,77±4,13	38,75±4,21	38,75±4,41
34,42	40,06±4,33	40,50±5,42	37,62±2,87	38,99±4,00	38,47±4,09	38,61±4,12
29,72	44,32±5,82	44,42±4,95	43,49±5,50	43,16±4,95	43,59±4,98	43,23±4,44
25,10	49,87±5,55	50,11±5,85	49,22±5,72	46,646±5,56	47,16±5,48	46,14±4,87
20,35	55,09±6,24	55,05±6,40	54,62±6,13	51,86±6,54	51,70±5,79	51,35±5,81
11,01	64,61±11,07	64,93±9,95	69,35±9,96	63,68 ±9,75	64,87±8,38	62,08±7,95

Table 6. Values of the lifetime and standard deviation for the imaging method.

Method	Layer cover	SPOT	Linear fit
Phase-angle method	PS (BOTTOM)	1	y = -0,8009x + 71,146
		2	y = -0,8065x + 72,142
		3	y = -0,7597x + 70,204
	TiO2 in E4 (TOP)	1	y = -1,0606x + 76,561
		2	y = -1,0602x + 76,767
		3	y = -1,0232x + 75,481
Imaging method	PS (BOTTOM)	1	y= -0,8775x + 70,755
		2	y= -0,9045x + 71,695
		3	y= -0,8535x + 69,447
	TiO2 in E4 (TOP)	1	y= -1,667x + 79,935
		2	y= -1,1063x + 78,296
		3	y= -1,1458x + 79,183

Table 7. Linear fit for each of the spots of the PdDBADCB in PViCl with the different measurement methods.

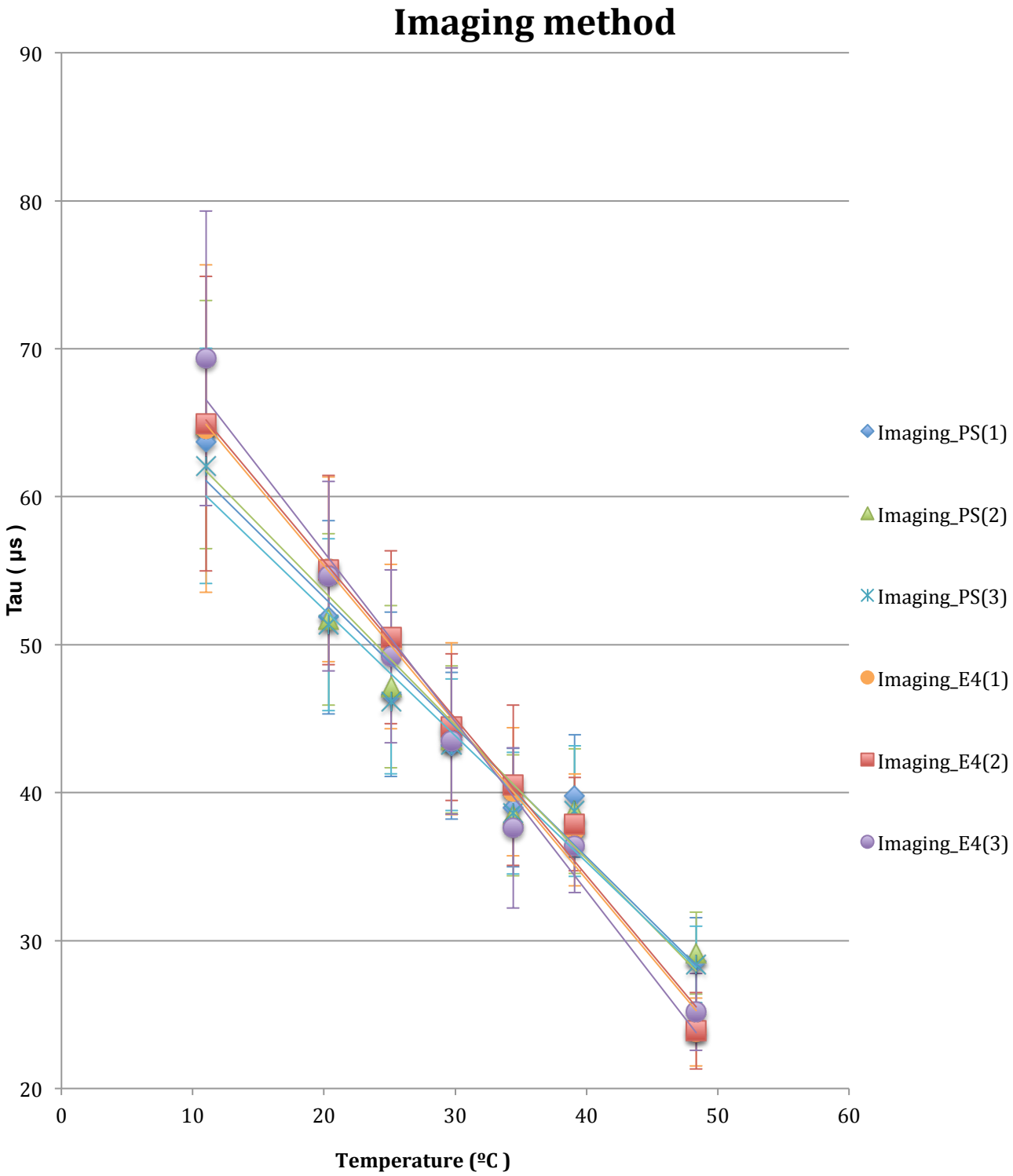

Figure 17. Lifetime and standard deviations obtained of the PdDBADCB in PViCl-PAN with the different layer covers for the different spots and temperatures with the time-domain/imaging method.

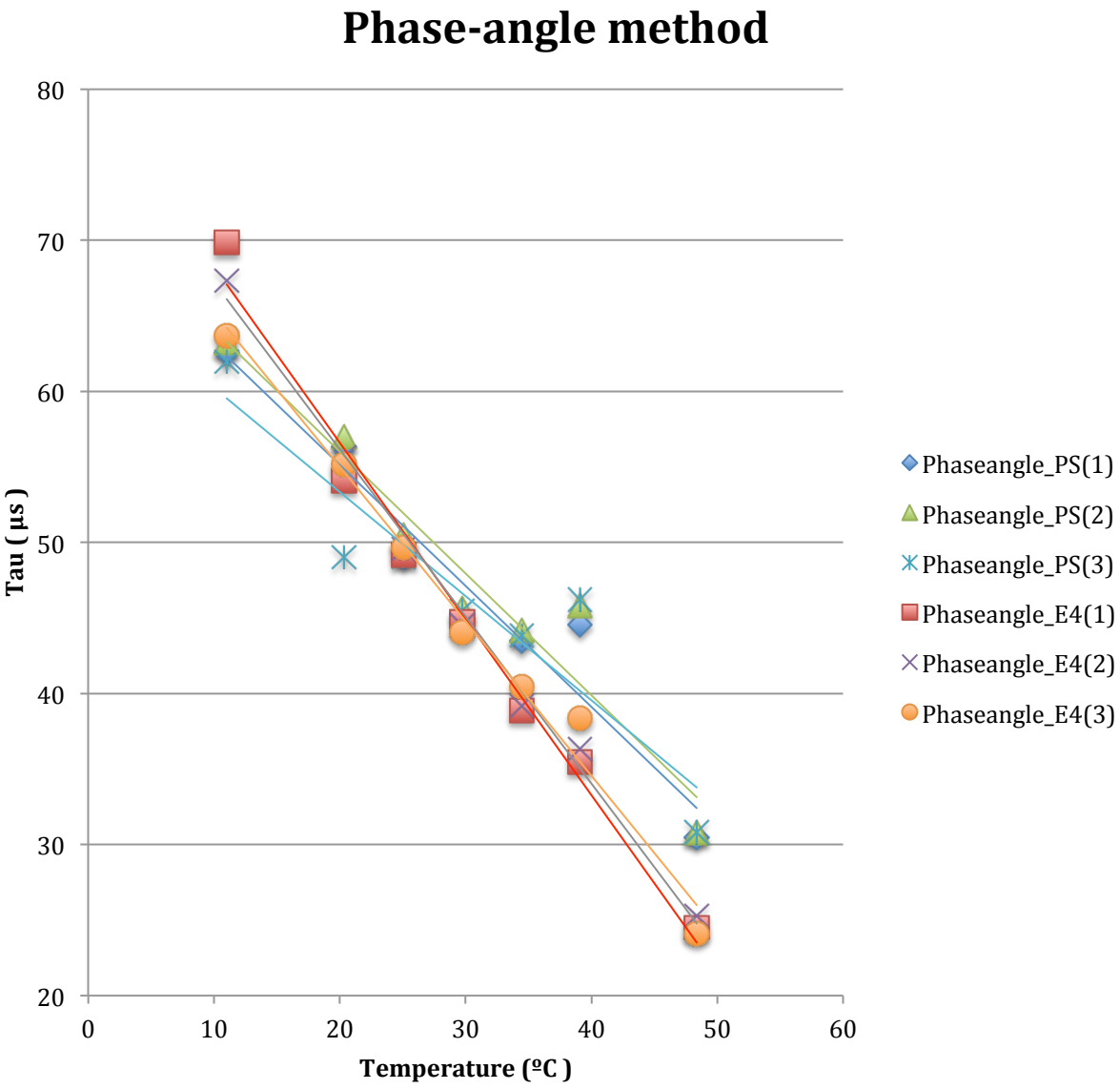

Figure 18. Lifetime and standard deviations obtained of the PdDBADCB in PViCl-PAN with the different layer covers for the different spots and temperatures with the frequency-domain/phase-angle method.

From now on, the aim is to see if there exists some temperature gradient along the chip taking into consideration the different flowrates. Presumably, as the speed of the water increases, it is expectable a higher temperature difference between the spots, since there is less time for the water to be warmed. The water is pumped into the chip at a normal room temperature and it is warmed with the heater when it enters in the chip.

With the increase of the flow rate, the initial spot is expected to have lower temperatures than the last one on the circuit.

Regarding the temperatures expected for the top and the bottom of the chip, with the phase-angle method, except for the 2,5 µl/min flowrate and the value of the third spot for the 500 µl/min flowrate, all the others flowrates show normal result, **Table 9** and **Figures 19-22.** This means that the

temperature on the top is lower than the temperature on the bottom. Nevertheless, with the imaging method there must have been some kind of error because there can be seen unexpected results for all the flowrates. In all of them, the temperature on the top of the chip is higher than the temperature on the bottom, which at first sight doesn't make any sense. This might be explained with the standard deviation of the imaging method by the calibration; with such high values of standard deviation we can't conclude anything about the results obtained and the difference between top and bottom.

It is important to highlight that syringe pumps's main drawbacks are that they develop pulsatile flows at low flow rates and that the time required to stabilize its effective flow rates is to large. These two conditions may be involved in the results obtained for the flow rate of 2,5 µl/min, since the results may have been distorted by not waiting long enough or by pulsating flows.

Focusing on the values obtained for the different flowrates, it can be seen that for 2,5 µL/min and 25 µL/min with the phase-angle method it is difficult to detect a temperature gradient between the equidistant spots, **Figure 19** and **20**. With 500 µL/min it is obvious that there is a temperature gradient, visible in one method as in the other, **Figure 22**.

Usually, in the experiments that implicate cell culture, researchers work with shear forces of 10 µL/min*mm^2 on the chips. Taking into consideration the critical dimension of the channel of the chip, the estimation of the flowrate to achieve this value is made. With 75 µL/min, **Figure 20**, is possible to detect a temperature gradient with the phase-angle method.

The calculated shear forces for the different flow rates are:

- 2,5 (µL/min): 0,35 µL/min*mm^2
- 25 (µL/min): 3,5 µL/min*mm^2
- 75 (µL/min): 10,6 µL/min*mm^2
- 500 (µL/min): 71 µL/min*mm^2

Dismissing the results obtained by the imaging method, then it can be concluded that the top and the bottom temperatures are generally the expected ones and that even with flows of 75 µL/min the chip starts to present some temperature gradient. Anyway, the value obtained for the flow rate of 2,5 µL/min makes us question the validity and degree of error of the rest of the results obtained.

.

Flow rate (µL/min)		Pos. 1	Pos. 2	Pos. 3
2,5	TOP	36,25	37,45	37,49
	BOTTOM	35,06	35,11	35,25
25	TOP	35,29	35,22	34,99
	BOTTOM	36,28	37,37	37,2
75	TOP	34,00	34,73	34,76
	BOTTOM	34,52	36,35	36,28
500	TOP	24,94	31,56	34,73
	BOTTOM	26,84	32,88	32,66

Table 9. Temperatures obtained by the phase-angle method for the different spots of the chip.

Flow rate (µL/min)		Pos. 1	Pos. 2	Pos. 3
2,5	TOP	35,1	37,13	35,24
	BOTTOM	34,35	34,59	33,71
25	TOP	35,73	36,07	35,46
	BOTTOM	34,31	34,16	34,11
75	TOP	35,03	35,33	35,12
	BOTTOM	35,96	35,31	35,2
500	TOP	26,58	31,66	33,47
	BOTTOM	26,69	28,84	33,18

Table 10. Temperatures obtained by the imaging method for the different spots of the chip.

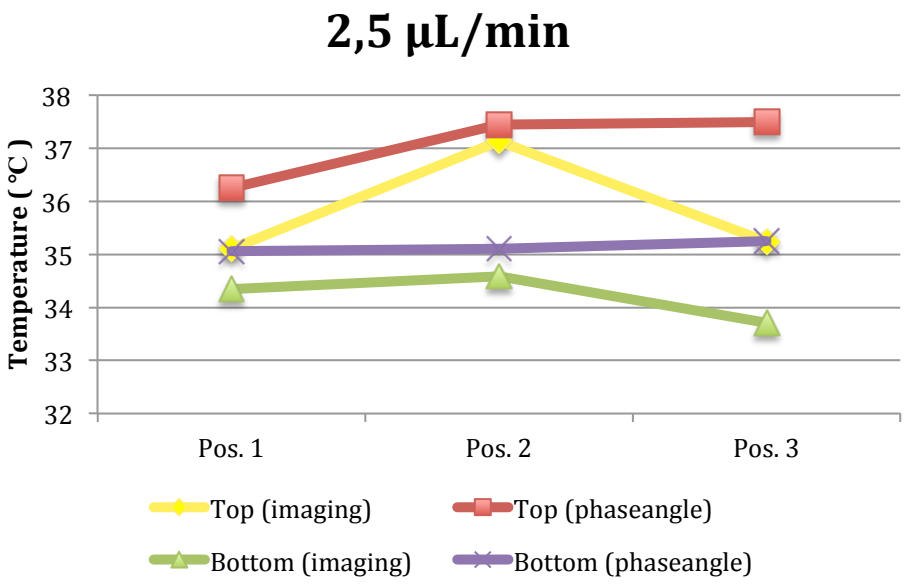

Figure 19. Temperature measured on the 3 equidistant spots for each layer cover at a flowrate of 2,5 µL/min.

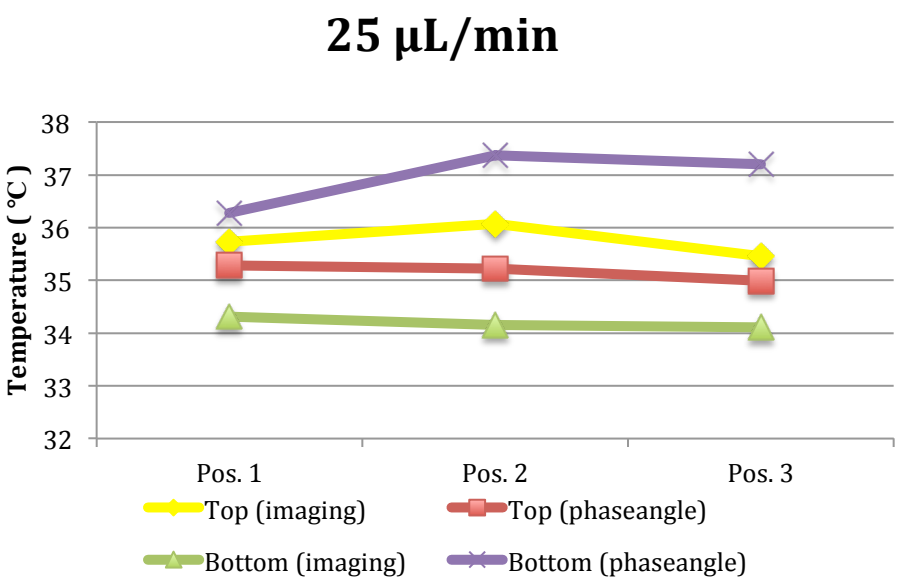

Figure 20. Temperature measured on the 3 equidistant spots for each layer cover at a flowrate of 25 µL/min.

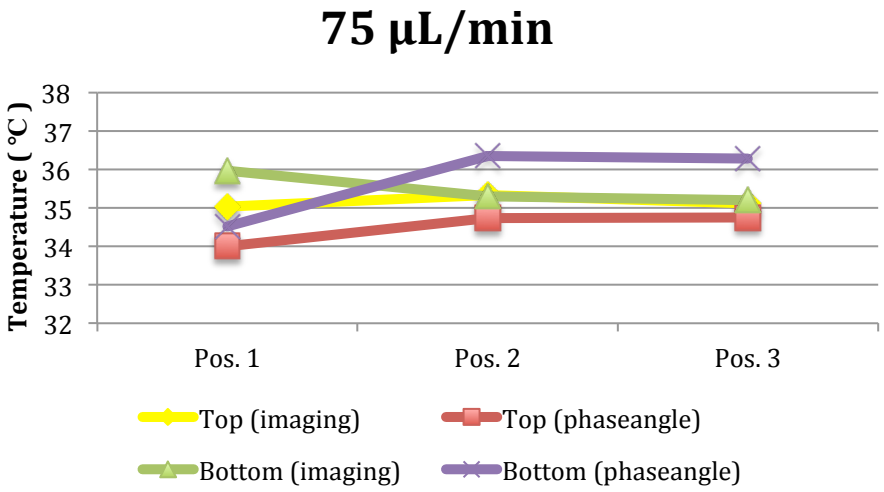

Figure 21. Temperature measured on the 3 equidistant spots for each layer cover at a flowrate of 75 µL/min.

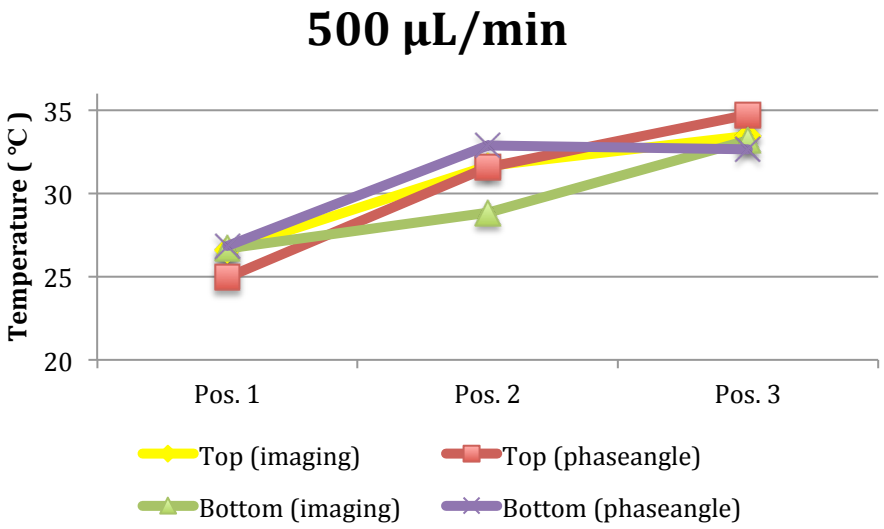

Figure 22. Temperature measured on the 3 equidistant spots for each layer cover at a flowrate of 500 µL/min.

Conclusions

Measuring temperature precisely is very difficult, even when working with methods that have the same theoretical basis, in practice the results obtained can vary between the imaging method and the phase-angle method.

The temperature dependent luminescence emission of the different dyes was investigated in the temperature range from 10 °C to 50 °C. The dyes show different sensitivities to temperature, but all of them present a decrease of lifetime with its increase. Specifically, the Pd dye based sensing material stood out in front of the other materials for its capacity and precision for the measurement of temperature.

Beyond the selection of the material, this work focused on checking from what flowrates changes of temperature could be perceived along a microfluidic chip. It was verified that for flowrates normally used in experiments carried out with this type of chips (75 µL/min), temperature gradients were already detected. It is inecessary to mention that the extraction of these conclusions is subject to certain error due to the results obtained for the lowest flow rate, for which no underlying explanation was found.

For researching it is of remarkable importance to know in which conditions an experiment is being carried out and consider all the variables. In the case of chips involved in cell culture, any variation could involve abrupt changes.

It is important to continue investigating on and developing this field since this type of temperature measurement could be the future for biomedical research. It could lead us to measurements in the intracellular-body, which would signify a great advance because temperature is one of the most significant variables for knowing what is happening inside the cell.

Outlook

Possible suggestions for carrying out these experiments on the future for further research could be the use of smaller channels or trying out to get the imaging of the whole channel instead of only the different spots. It would also have been interesting to implement the chip experiment with flow rates between 75 μL/min and 500 μL/min to see how the gradient increases as the flowrate augments.

For future experiments it also would be advisable not to maintain the thermal insulation cover during the experiment with different flow rates, since in regular cell experiments it is not possible to use it.

References

[1] K. Okabe, N. Inada, C. Gota, Y. Harada, T. Funatsu & Seiichi Uchiyama, Nat. Commun., 2012, 3, 705.
[2] X. Wang, O. S. Wolfbeis, R. J. Meier, Chem. Soc. Rev. 2013, 42, 7834.
[3] L. Michalski, K. Eckersdorf, J. Kucharski, J. McGhee, in Temperature Measurement, John Wiley & Sons, Ltd, Chichester, UK, 2002, pp. 1–18.
[4] J. Gershon-Cohen, Ann N Y Acad. Sci., 1984, 121, 4.
[5] C. Wang, R. Xu, W. Tian, X. Jiang, Z. Cui, M. Wang, H. Sun, K. Fang, N. Gu, Cell Res. 2011, 21, 1517.
[6] C. D. S. Brites, P. P. Lima, N. J. O. Silva, A. Millán, V. S. Amaral, F. Palacio, L. D. Carlos, Nanoscale 2012, 4, 4799.
[7] D. J. Griffiths, Introduction to Quantum Mechanics, Prentice Hall, 2004.
[8] J. R. Lakowicz, Principles of Fluorescence Spectroscopy., Kluwer Academic / Plenum Publishers, 1999.
[9] K. A. Franz, W. G. Kehr, A. Siggel, J. Wieczoreck, W. Adam, "Luminescent Materials" in Ullmann's Encyclopedia of Industrial Chemistry, Wiley-VCH, 2002.
[10] D. Hu, L. Yao, B. Yang, Y. Ma, Philos. T. Roy. Soc. A, 2015, 373, 2044.
[11] K. Suhling, L. M. Hirvonen, J. A. Levitt, P. H. Chung, C. Tregidgo, A. Le Marois, D. A. Rusakov, K. Zheng, S. Ameer-Beg, S. Poland, S. Coelho,R. Henderson, N. Krstajic, Med. Photonics, 2015, 27, 3.
[12] M. Schäferling, Angew. Chem. Int. Ed., 2012, 51, 3532.
[13] H. Uoyama, K. Goushi, K. Shizu, H. Nomura, C. Adachi, Nature 2012, 492, 234.
[14] Q. Zhang, H. Kuwabara, W. J. Potscavage, S. Huang, Y. Hatae, T. Shibata, C. Adachi, J. Am. Chem. Soc. 2014, 136, 18070.
[15] F. Venturini, M. Baumgartner, S. M. Borisov , Sensors, 2018, 18, 668.
[16] G. Accorsi, G. Verri, M. Bolognesi, N. Armaroli, C. Clementi, C. Miliani, A. Romanic, ChemComm, 2009, 23, 3392.
[17] A. Steinegger, I. Klimant, S. M. Borisov, Adv. Optical Mater. , 2017, 5, 1700372.
[18] S. M. Borisov, R. Pommer, J. Svec, S. Peters, V. Novakova, I. Klimant, New Red-Emitting Schiff Base Chelates: Promising Dyes for Sensing and Imaging of Temperature and Oxygen via Phosphorescence Decay Time, Non-published.